

Design of a MEMS Capacitive Comb-drive Accelerometer

Tolga Kaya*¹, Behrouz Shiari², Kevin Petsch¹ and David Yates²

¹Central Michigan University, ²University of Michigan

* kaya2t@cmich.edu

Abstract: This work describes of a novel, three-direction MEMS capacitive accelerometer for health monitoring applications. COMSOL Multiphysics was used to study the working principle and the dynamic performance of the accelerometer. In the first step, the motion of the proof-mass was investigated by coupling the squeeze-film gas damping to the structural dynamic of the accelerometer. The modified Reynolds equation for perforated plate was implemented into COMSOL model to capture the proof-mass out-of-plane deflection. The maximum design acceleration was considered 5g in all directions. The magnitudes of von-mises stresses in the serpentine springs were calculated for the predictions of fracture failures under maximum design acceleration and deflections. A modal analysis was also used to find the fundamental modes of vibration and frequencies, in order to avoid resonance and identify the device range of operation. At the end, a series of three-dimensional electrostatic finite element analysis was conducted to calculate the mutual capacitance between the moving and fixed fingers when the proof-mass is subjected to an in-plane design acceleration.

Keywords: Accelerometer, Gas-damping, Finite Element, Capacitive, Electrostatic.

1. Introduction

Over the last decade, extensive efforts have been devoted to the development of micro-accelerometers for different applications such as automotive safety, navigation, audio-video and health monitoring. Many of these applications stand to benefit from MEMS accelerometer that have an excellent sensitivity and a wide dynamic range while still being low cost and mass produced [1-3].

There are many different ways to make an accelerometer. The physical mechanisms underlying MEMS accelerometers include piezoresistive, electromagnetic, piezoelectric, ferroelectric, optical, tunneling, thermal, electrostatic and capacitive. This article is focused on the latter.

The MEMS capacitive accelerometer design has the advantage of smaller size, weight, and reduced parasitics due to single-chip integration. Capacitive sensing is independent of the base material and relies on the variation of capacitance when the geometry of a capacitor is changing. They have excellent sensitivity and the transduction mechanism is intrinsically insensitive to temperature [4-5].

Comb-drive accelerometer usually consists of two finger structures, called fixed finger and movable finger. The fixed fingers are fixed to the accelerometer frame. The movable fingers are attached to a proof-mass and suspended by flexible elements to the frame. The device senses any external acceleration which is transferred to the proof-mass through the flexible elements such as springs. The proof-mass and movable fingers move along the direction of body force, the fixed comb remains stationary. This movement changes the capacitance between the fixed finger and the movable finger. The capacitance is measured using electronic circuitry [6].

In general, MEMS accelerometers fabrication relies more on trial-and-error than on clear design principles. Since the trial-and-error basis fabrication and testing of MEMS are extremely costly, comprehensive modeling and simulation can be a valuable tool to evaluate different designs, perform parametric studies and virtual prototype each MEMS design before actual fabrication [7].

This work presents a MEMS capacitive comb-drive accelerometer with three sensitive directions. The device is designed for health monitoring applications. The accelerometer has different sensitivity in different axes. The proof-mass of the device is suspended by four serpentine springs, and the comb-drive structure is used to form the differential capacitor to measure the displacement of the proof-mass as shown in Figure 1. This combination forms a mechanical oscillator with specific resonance frequency. The structure has an area of 2 mm × 2 mm and a thickness of 0.1 mm. The suspended proof-mass is perforated by 49; 20µm x 20µm etch-release holes.

COMSOL Multiphysics is used to study the working principle and dynamic performance of the MEMS capacitive accelerometer with the comb drive structure. Different concept designs were virtually tested in order to establish a final design with an understanding of its function prior to fabrication. Among various designs, the final structure was selected as shown in Figure 1.

This paper will briefly cover several finite element modeling and analysis steps to clarify the advantages and disadvantages of the design. Finally, the relevant conclusions will be drawn from this effort.

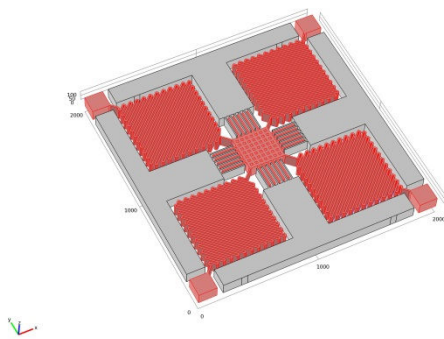


Figure 1. Capacitive comb-drive accelerometer.

2. Dynamics of the Device

In our accelerometer, inertia produces a motion that the device detects. As shown in Fig. 1, the device acts as a mechanical oscillator with a specific resonance frequency. However, in accurate motion-detection applications these resonances are unwanted, and the device damps the movements to produce smooth time-step and frequency responses. Such a device can usually achieve suitable damping with a low gas pressure that, considering the dimensions of the device, leads to rarefied gas effect in the system.

A narrow gap formed by two solid parallel flat parts of the accelerometer constrains the displacement of the air perpendicular to the surfaces. When the proof-mass squeezes the gap, the gas flows out from its edges and holes. The narrow pathway restricts the flow, which causes gas pressure to increase. This increase in gas pressure, in turn, decelerates the proof-mass movement.

Modeling squeezed involves coupling the modified Reynolds equation with the equations

for the structural displacements. The proof-mass of the accelerometer is perforated as shown in Figure 2. The plate has 49 holes. To consider the presence of the holes in the out-of-plane motion of the proof-mass, the pressure distribution in the model is replaced by the modified Reynolds equation for perforated plate [8]. This form of the modified Reynolds equation originally was not present in the software. Therefore it was inserted into it thereby expanding the capabilities of the software. Then, the model considers the solid moving parts in the accelerometer using the solid mechanics physics interface in 3D and the squeeze-film air damping on the lower and upper surfaces using the Film-Damping Shell physics interface.

The accelerator geometry was designed using AutoCAD software and then imported into COMSOL. The structure of the device was geometrically simplified by considering only the moving parts of the accelerometer shown in Figure 1 to reduce computation time. The model consists of only silicon proof-mass and four serpentine springs. The springs were fixed at their ends. The external acceleration was modeled as body force. The total simulation time was considered 4 ms and the time step was set to 0.01 ms. The moving parts of the accelerometer were subjected to 5g threshold acceleration in direction x (in-plane) and direction z (out-of-plane) in all simulations. A 3D tetrahedral element, 10 node, size-varying mesh was used in all simulations.

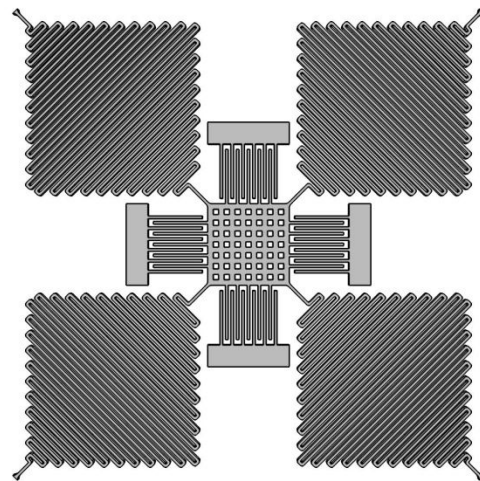


Figure 2. Simplified CAD model of the capacitive accelerometer.

Material properties and geometrical parameters of the accelerometer are listed in Table 1.

Table 1: Material properties and geometrical parameters used in all conducted simulations. Mean free path of air is taken from [7].

Parameter	Value	Unit
Area of Accelerometer	2000×2000	μm^2
Area of proof-mass	395×395	μm^2
Thickness of proof-mass	100	μm
Young modulus of silicon	1.67×10^{11}	N/m^2
Poisson ratio of the silicon	0.3	
Density of Silicon	2300	Kg/m^3
Relative permittivity of silicon	11.9	
Viscosity of air at 25°	1.1839×10^{-5}	Pa.s
Mean free path of air at 25°	6.78×10^{-8}	m
Relative permittivity of air	1	

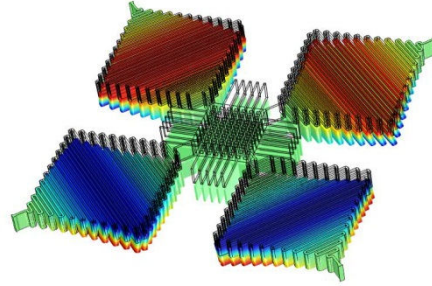


Figure 4. Profile of maximum deformation of the proof-mass and serpentine springs in z direction.

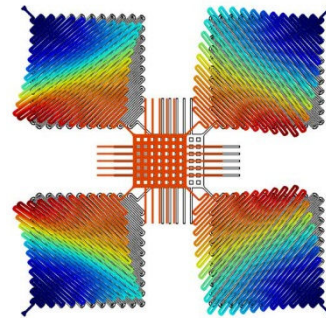


Figure 5. Profile of maximum deformation of the proof-mass and serpentine springs in x direction.

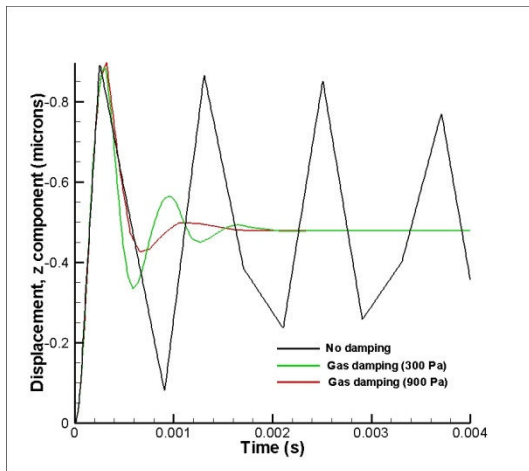


Figure 3. The z displacement of the proof-mass center at 0 Pa, 300 Pa, and 900 Pa ambient pressure, respectively.

Figure 3 shows the z displacement of the proof-mass center as a function of time for ambient pressures of 0 Pa (or no-damping), 300 Pa, and 900 Pa, respectively. As ambient pressure increases, the film damping at the upper and lower surfaces increases through the increase in the air effective viscosity and density. This increased damping results in a substantial decrease in oscillation with increasing pressure. At 900 Pa, there is no apparent oscillation after the first overshoot, and the proof-mass seems asymptotically reaching the value of 0.5 micron deflection in z direction.

Figure 4 shows the deformation of the moving parts of the accelerometer at 0.25 ms. The maximum deflection of the middle of the proof-mass is almost 0.9 microns. This maximum deflection is an important factor in the out-of-plane sensing of the device.

Figure 5 shows the deformation of the proof-mass and four springs at 0.5 ms. The maximum deflection of the proof-mass center is almost 1.4 microns. This maximum is also will dictate the maximum output of the device for in-plane sensing.

Polycrystalline silicon shows an excellent flexibility at the micro-scale and resists very high rate body forces. In the designed accelerometer, all serpentine springs made of silicon still need to be carefully designed to prevent fracture. If a spring is broken during the operation, the device will not work anymore. As shown in Figure 6, the maximum von-mises stress occurs at the deformed curved corners of the springs close the fixed ends. The maximum stress at the critical zones was lower than 2 Mpa. Since fracture stress for single crystal silicon is 7 GPa, the result show that the device can survive under a 5g applied acceleration in both x and z directions.

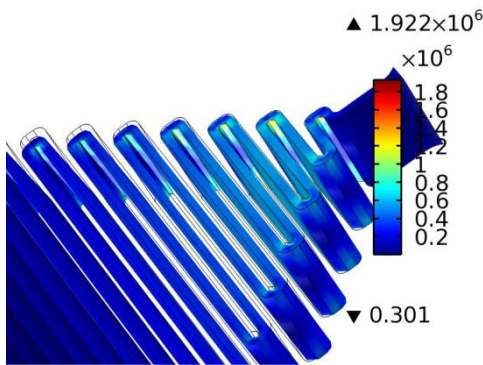


Figure 6. Contour of von-mises stress at the curved sections of the serpentine spring. The applied acceleration is in z direction.

3. Modal Analysis of the Device

Lowering the spring stiffness to achieve more deflection in the capacitive comb-drive accelerometer always results a lower resonance frequency. This is the trade-off in performance of the accelerometer. A rule of thumb is that an accelerometer is usable up to about 1/3 of its lowest natural frequency. The collected data above this frequency will be accentuated by the resonant response, but may be used if the effect is taken into consideration.

A modal analysis was conducted to calculate the fundamental frequencies and modal shapes of the accelerometer. The boundary condition applied included four anchors constrained in all directions. The resonant frequencies obtained are shown in Table 2. The lowest frequency was in the x (or y) axis. The mode shape at this low frequency is shown Figure 7. The third mode is an out-of-plane and it happens at 1838 Hz. The rotational vibration of the proof-mass along the z-axis happens at 1955.

Table 2: Resonant frequencies and mode shapes

Order	Resonant frequency (Hz)	Mode shapes
1&2	1280	Vibrating by x or y axis (In-plane mode)
3	1838	Vibrating in z axis (out-of-plane mode)
4	1953	Vibrating along z axis (rotational mode)
5	39105	Vibrating along y or x axis (rotational mode)

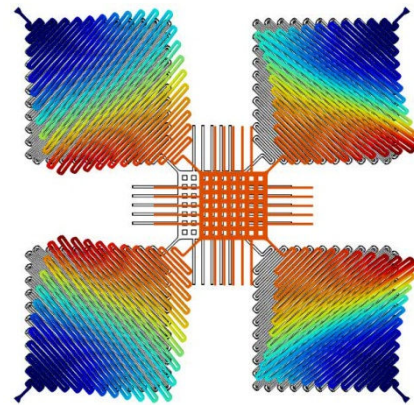


Figure 7. Mode at 1280 Hz. The vibration happens by x-axes.

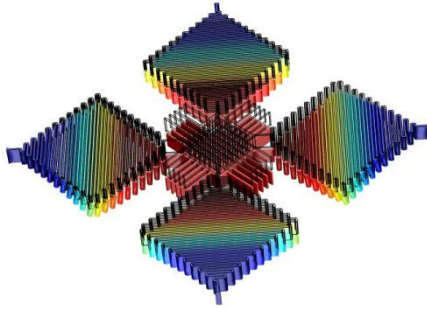


Figure 8. Mode at 1838 Hz. The vibration happens by z-axes.

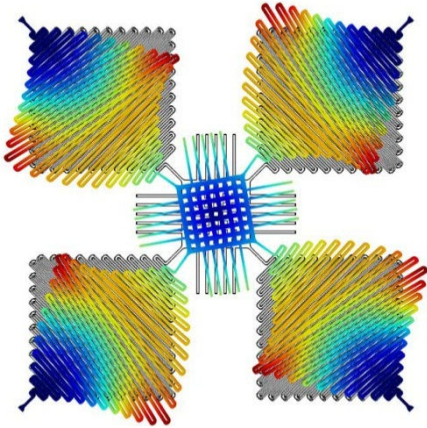


Figure 9. Mode at 1953 Hz. Vibration happens along z-axis

4. Electrostatic Modeling

Deflection of the proof-mass due to externally applied acceleration can be measured using a differential capacitor. The differential capacitor involves the interdigitation of moving fingers attached to the proof mass with fixed fingers attached to the frame. The differential capacitance is proportional to the overlapping area and the distance between the moving and fixed fingers. With the capacitor area fixed by the fabrication process, the differential capacitance and hence the circuit output voltage is proportional to the difference between gaps in the right and left side of each finger, as shown in Figure 10.

In order to test the efficiency of the design in producing appropriate outputs during the operation, a series of electrostatic simulations were carried out by only considering a pair of combs for sensing acceleration in y direction as shown in Figure 10. The combs were modeled as three-dimensional solids surrounded and separated by air dielectric. Figure 10 also shows the model dimensions and mesh sizes that are altered for ease of viewing the center fingers inside the air box.

The moving fingers (red section in Figure 7) were shifted in y direction from 0.25 to 2.5 micron in an iterative solving process. The capacitance was calculated using the energy-storage distribution in the electric field and integrating over the volumetric domain in each shifting step.

The plot of capacitance versus the moving distance of the comb is shown in Figure 11. Based on the simulation results in section 2, the capacitance value correlated to maximum deflection of the proof mass in y direction is 0.208 pF.

The simulated electrical potential distribution for the comb capacitors under the displacement of 1.2 μm are shown in Figure 12.

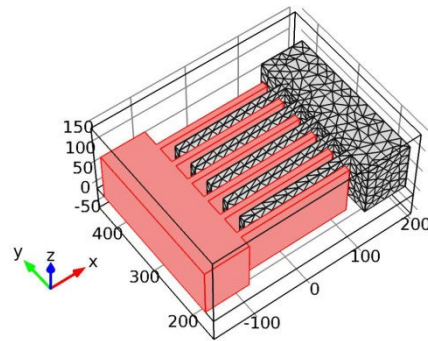


Figure 10. A pair of combs for capacitance-based measuring of acceleration in y direction. The combs are surrounded with air.

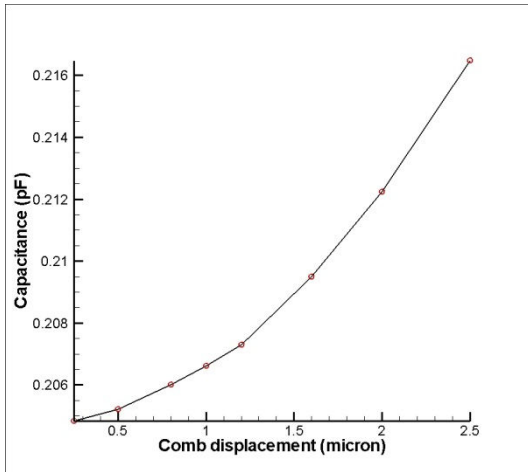


Figure 12. Plot of the capacitance versus the moving comb displacement in y direction.

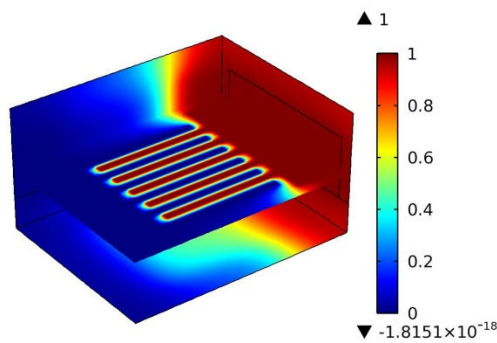


Figure 11. Electrical potential of the surface of the combs.

5. Conclusions

In this paper, the dynamic and performance of a MEMS comb accelerometer is studied. A modified squeeze-film gas damping model for perforated plates is implemented in COMSOL to calculate the proof-mass out-of-plane deflection under 5g acceleration. Based on the numerical results, low gas pressure (900 Pa) leads to a smooth frequency response of the accelerometer. The simulation results also show that the intensity of the serpentine springs which is the weakest part in the accelerometer meets the material intensity under the applied external accelerations in all directions. A modal analysis was used to extract the fundamental frequencies and modal shapes of the design as a reference for the range of operation of the device. The lowest

natural frequency of the device is about 1.3 KHz. A series of three-dimensional electrostatic finite element analysis is conducted to calculate the mutual capacitance between the moving and fixed fingers of the combs. The results can be used to calculate the accelerometer outputs and possible modifications of the comb structures in the future.

6. References

1. G A MacDonald, A review on low cost accelerometers for vehicle dynamics, *Sensors and Actuators*, **A21-A23**, 303-307 (1990)
2. R Legtenberg, A W Groeneveld and M Elwenspoek, A high-sensitivity z-axis capacitive silicon microaccelerometer with a torsional suspension, *Journal of Microelectromechanical Systems*, **7**, 192-200 (1998)
3. R Legtenberg, A W Groeneveld and M Elwenspoek, Combdrive actuators for large displacements, *Journal of Micromechanics and Microengineering*, **6**, 320-329 (1996)
4. H. Xie and G. Fedder, A CMOS Z-axis capacitive accelerometer with comb-finger sensing, *Proceedings of the 13th IEEE International Conference on Micro Electro Mechanical Systems*, 496-501 (2000)
5. Wan-Chun Chuang, Hsin-Li Lee, Pei-Zen Chang and Yuh-Chung Hu, Review on the modeling of electrostatic MEMS, *Sensors*, **10**, 6149-6171, (2010)
6. S D Senturia, R M Harris, B P Johnson, S K Nabors, M A Shulman, and J K White, A computer-aided design system for microelectromechanical systems (MEMCAD), *Journal of Microelectromechanical Systems*, **1**, 3-13, (1992)
7. S G Jennings, The mean free path in air, *Aerosol Sci.*, **19**, 159-166 (1988)
8. M Bao, H Yang, Y Sun, and P J French, Modified Reynolds equation and analytical analysis of squeeze-film air damping of perforated structures, *J. Micromech. Microeng.*, **13**, 795-800 (2003)

7. Acknowledgements

We acknowledge the National Nanotechnology Infrastructure Network Computation project, NNIN/C, at Michigan for computational resources.